J Solid State Electrochem (2007) 11:1043–1050
DOI 10.1007/s10008-007-0266-8

ORIGINAL PAPER

Viscoelastic phenomena during electrochemical deposition of polyaniline films

Mohamoud A. Mohamoud · A. Robert Hillman

Received: 22 August 2006 / Revised: 11 October 2006 / Accepted: 12 October 2006 / Published online: 7 February 2007

Abstract Electrochemical quartz crystal microbalance (EQCM) and crystal admittance measurements were used to study the potentiodynamic electrodeposition of polyaniline films. Variations in peak admittance provided the distinction between acoustically thin and acoustically thick films. In the former instance, the Sauerbrey equation was used to interpret the EQCM frequency shift in gravimetric terms. In the latter case, admittance spectra were interpreted viscoelastically to yield shear storage and loss moduli. Variations in storage modulus with potential (within a given deposition cycle) and with number of deposition cycles (at a given potential) were small, covering the range 1.1–1.6 × 10^7 dyn cm^{-2}. Variations in loss modulus were much more dramatic, increasing from very low levels typical of a simple fluid to values similar to the storage modulus. More subtle variations of both components within a single potential cycle were highlighted using a novel differential format. This revealed two peaks, correlating with the first film redox process and with further film oxidation/polymerization.

Keywords Viscoelasticity · Shear modulus · Polyaniline · Conducting polymer · Acoustic wave device · Quartz crystal microbalance

Contribution to the International Workshop on Electrochemistry of Electroactive Materials (WEEM-2006), Repino, Russia, 24–29 June 2006.

M. A. Mohamoud · A. R. Hillman (✉)
Department of Chemistry, University of Leicester,
University Road,
Leicester LE1 7RH, UK
e-mail: arh7@le.ac.uk

Introduction

Polyaniline is one of the most widely studied and important conducting polymers [1–6]. Accordingly, the electrochemical [5, 7], optical [4, 8] and chemical [9] properties, several aspects of polymer structure [3, 10–13] and the dynamics of redox switching and the associated ion transfers [3, 7, 12, 14–17] have been studied in some detail. However, relatively little attention has been paid to the viscoelastic properties of polyaniline films. Following the acquisition of useful insights of this nature for polypyrrole [18] and several polythiophene-based [19–22] films, we, therefore, now focus on this component of film dynamics for polyaniline. In this report, we focus, particularly, on the evolution of film viscoelastic properties during film deposition.

An understanding of film viscoelastic properties is important in a fundamental sense, as its absence makes any appreciation of the relationship between polymer composition, structure and dynamics incomplete. It also has practical significance, as the motions—on local or more extended distance scales—of the polymer chains control the effective viscosity of the medium and, thereby, the diffusion of mobile species. The transport rates of these latter species (ions, solvent, reactant) are key determinants of device performance in virtually all practical applications.

Studies of the morphology of polyaniline at different stages during film growth suggest that two of the more important parameters are the background electrolyte concentration and the identity of the anion present during film deposition [11, 23]. On the basis of scanning electron microscope (SEM) images of polyaniline film surfaces [3, 11] and electrochemical quartz crystal microbalance (EQCM) data [3, 11, 12], it has been proposed that one can categorize anions into two classes, according to their effect on film morphology. The so-called class 1 anions

(BF_4^-, ClO_4^- and $CF_3CO_2^-$) promote a compact film structure, whereas the so-called class 2 anions (SO_4^{2-}, NO_3^- and Cl^-) promote an open film structure [11]. The ex situ SEM images of films prepared in the presence of these two types of anion clearly show different levels and distribution of void space, which one would reasonably expect to be filled with solvent in situ. Given the quite general effect of solvent as a plasticiser, this in turn would give an expectation of different film viscoelastic properties.

To our knowledge, this is the first time that viscoelastic data have been reported for polyaniline film electrodeposition. The general strategy is to use a high frequency acoustic wave device (a thickness shear mode, TSM, resonator) to provide the surface mechanical impedance, from which we can extract the film mechanical behaviour. This is generally parameterized in terms of the shear modulus (G), expressed as the complex quantity $G'+jG''$, where G' is the storage modulus, G'' is the loss modulus and j indicates the phase relationship. In this report, we focus on the evolution of G during film deposition; a future communication will focus on the related, but separate, matter of the subsequent response of G to film redox cycling in the absence of monomer in solution. Ultimately, the value of G and its response to external stimuli are manifestations of the underlying molecular dynamics.

Experimental

Materials

Aniline (99+%, Lancaster) and $HClO_4$ (60%, BDH) were used as received. A freshly prepared sample of aqueous 0.1 M aniline/1 M $HClO_4$ was used for each film deposition experiment.

Instrumentation

The EQCM and crystal impedance instrumentation have been described in detail elsewhere [24–26]. The working electrode was an Au thin film supported on a polished AT-cut 10-MHz quartz crystal (International Crystal Manufacturing, Oklahoma City, USA), with electrochemically and piezoelectrically active areas, respectively, of A_e=0.23 and A_p=0.21 cm^2. The crystal was mounted at the bottom of a three-electrode conventional cell with silicone sealant (Dow Corning 3145 RTV) where one of the Au electrodes sandwiching the crystal acted as the working electrode. All potential measurements were made and are reported with respect to a home-constructed saturated calomel electrode as the reference electrode. The counter electrode was a Pt gauze. During polymer film deposition, crystal admittance spectra were acquired using a Hewlett-Packard HP8751A network analyser connected to a HP87512A transmission/reflection unit via a 50-Ω coaxial cable [17, 27, 28]. Electrochemical and acoustic wave device data collection were controlled via a computer running the HP VEE program and connected to the network analyser through an HP10833B interface card. The transmission/reflection unit was used to measure the scattering parameter, $S_{11}(f)$, as a function of frequency, f, in the vicinity of crystal resonance which returns the electrical input impedance, Z_s, of the thickness shear mode resonator as described below [27, 28]:

$$Z_s(f) = Z_0\left(\frac{1+S_{11}(f)}{1-S_{11}(f)}\right) \quad (1)$$

where Z_0 is the standard impedance of the system (here, 50 Ω).

Procedures

Polyaniline was deposited potentiodynamically ($-0.2 \leq E/V \leq 0.9$; v=10 mV s^{-1}) from aqueous 0.1 M aniline/1 M $HClO_4$ solution. Initial measurements on the bare crystal in air and in the deposition solution were used to acquire crystal and solution parameters, respectively [21]. All measurements were made at room temperature (20±2 °C).

As the potential was cycled, acoustic admittance spectra were recorded at 2 s (20 mV) intervals, as described above. For the purposes of determining film shear moduli with good precision, one requires significant acoustic damping within the film, although not to such an extent that the signal/noise ratio is compromised. In terms of physical parameters, the requirement [29] is an acoustic phase shift (φ) greater than 20° (below which the film is acoustically "thin") but below 90° (where complications associated with film resonance arise [30, 31]). When a shear acoustic wave of angular frequency ω (ω=2πf) is launched into a film of thickness h_f and density ρ_f, the acoustic phase shift across the film is related to the latter's viscoelastic properties by [21, 24]:

$$\varphi = \gamma h_f = \omega h_f \sqrt{\rho_f}\sqrt{\frac{1+G'/|G|}{2|G|}} \quad (2)$$

where we have made use of the standard algebraic relationships:

$$\sqrt{G} = \left(\frac{|G|+G'}{2}\right)^{1/2} + j\left(\frac{|G|+G'}{2}\right)^{1/2} \quad (3)$$

and

$$|G| = \left[(G')^2 + (G'')^2\right]^{1/2} \quad (4)$$

In more immediately accessible practical terms, this useful operating range can be qualitatively appraised by

visual identification of an admittance maximum that drops by more than about 10% but less than 80% from that associated with the bare Au electrode in solution. This can be accomplished by on-screen inspection of the admittance spectra as the experiment proceeds. Under the conditions employed, this corresponded to an experiment covering typically 25 voltammetric deposition cycles. At the end of this process, the working electrode was disconnected at the cathodic end of a deposition cycle.

Data fitting

Procedures for extraction of the storage and loss shear moduli have been discussed in detail elsewhere [21, 24, 26, 32]; these are based on fitting the elements of a lumped element (Butterworth van Dyke) equivalent electrical circuit to experimental data, here, obtained during film deposition. Quantitatively, values of G' and G'' were calculated with the help of the Maple standard package by fitting experimental impedance (Z) data using [26, 29, 32]:

$$Z = j\omega\rho_s + Z_f\left[\frac{Z_L\cosh(\gamma h_f) + Z_f\sinh(\gamma h_f)}{Z_f\cosh(\gamma h_f) + Z_L\sinh(\gamma h_f)}\right] \quad (5)$$

where Z_f is the characteristic mechanical impedance of the film, γ is the shear wave propagation constant in the film [28], and Z_L is the characteristic mechanical impedance of the background electrolyte solution (a semi-infinite Newtonian fluid) [21]. These parameters are expressed in terms of previously defined quantities by:

$$Z_f = (\rho_f G)^{1/2} \quad (6)$$

$$\gamma = j\omega/\nu_f = j\omega\left(\rho_f/G\right)^{1/2} \quad (7)$$

$$Z_L = \left(\frac{\omega\rho_L\eta_L}{2}\right)^{1/2}(1+j) \quad (8)$$

where ρ_L and η_L are the density and the viscosity of the solution, respectively, and ν_f is the acoustic wave velocity across the film. The first term on the right hand side of Eq. 5 corresponds to the surface mechanical impedance resulting from polymer trapped within surface features, i.e. surface roughness of the electrode. Such material behaves as a rigidly coupled ideal mass. For the purposes of determining film viscoelastic properties, the tactic is to minimise the effect of this term with respect to the second, viscoelastic term. This is accomplished by the use of polished crystals [21, 22, 32], for which the scale of the roughness (measured as about 5 nm by atomic force microscopy [AFM] for the crystals used here) is much smaller than the film thickness (typically 100–500 nm, see below).

An earlier approach we used to determine film viscoelastic properties from data in the acoustically thick regime was to make separate determination of film density, ρ_f, directly from the acoustically thin regime and to extrapolate a value of film thickness, h_f, from coulometric data in the acoustically thin regime [21, 24]. Fitting of the impedance data (two measurands) to Eq. 5 then yields a unique solution for the shear storage and loss moduli.

In the present case, we used this routine (which presumes film uniformity) as a checking procedure on an alternative approach we have developed more recently [33]. In doing so, it is worth noting that for relatively soft films in general, the shear modulus values are relatively insensitive to the film density. Furthermore, for the particular case of polyaniline, the monomer (ρ_M=1.02 g cm^{-3}) and solvent (ρ_S=1.0 g cm^{-3}) components have relatively similar densities, so there is negligible uncertainty in film density introduced by variations in film solvation; we used a film density of ρ_F=1.0 g cm^{-3}. In the present study, the value of film thickness was obtained by an optimization process, in which the allowable bounds of film thickness were constrained in three ways. First, a combination of the coulometrically determined molar coverage and the monomer density gives a lower (solvent-free) bound to film thickness, h_f^0. Second, systematic variation of h_f above h_f^0 reveals a restricted range within which real and positive values of G' are obtained. Simultaneous application of this consideration for G'' results in a narrow range of physically acceptable h_f values (note that, in the context of a single shot dynamic deposition experiment, we cannot repeat this as a function of harmonic number as we have done for film redox switching to further tighten the constraint [19]). From a practical perspective, recalling that the goal is to determine film shear moduli, we also find that the G' and G'' values vary very little across this allowed h_f range.

Two final tests of consistency were applied. At an experimental level, AFM images were taken to assess film thickness directly. At an interpretational level, the values of the shear modulus components were used to calculate the decay length, δ, of the shear acoustic wave in the propagation direction, perpendicular to the interface [21]:

$$\delta = 1/\gamma = \frac{1}{\omega\sqrt{\rho_f}}\sqrt{\frac{2|G|}{1-G'/|G|}} \quad (9)$$

When physically realistic solutions to the shear modulus components are obtainable, one would expect the film thickness to be more than 0.1δ. When acceptable signal/noise ratios are observed in the raw spectra, one would expect $h_f<2\delta$, as the round trip (to the outer film interface and back to the electrode) for the acoustic wave is then 4δ, and the amplitude of the reflected wave is less than 2% of that for the outgoing wave.

Results and discussion

Qualitative overview of film deposition

Figure 1 shows the raw data for polyaniline film deposition from 0.1 M aniline/1 M $HClO_4$. Voltammetric current data were taken for all cycles and admittance spectra were acquired at 20 mV intervals throughout the experiment, but for clarity we only show selected responses. Panel a shows the *i*–*E* responses for cycles 5, 10, 15 and 20, representing different stages of the film growth. Using fresh solution for each experiment, these were reproducible and similar to those reported in the literature [3, 4, 34]. Admittance spectra are shown for the extreme negative (E=−0.2 V; panel b) and positive (E=0.9 V; panel c) ends of the scans.

Qualitatively, the trends in resonant peak admittance values in panel b (reduced film state) and panel c (oxidised film state) are of progressive damping as the film grows. For small numbers of deposition cycles, typically 1–3, the total damping in the system is very similar to that for the immersed bare electrode before initiation of electropolymerization. This corresponds to the presence of an acoustically thin film, for which the EQCM response is gravimetrically interpretable, according to the Sauerbrey equation (see below). Beyond five deposition cycles, the additional damping associated with electropolymerization is substantial: this corresponds to an acoustically thick film, for which the EQCM response is viscoelastically interpretable, according to Eq. 5. One final point that is just about visually discernable from detailed comparison of panels b and c is that the magnitude of the peak admittance with the film in the oxidised form is slightly higher than that for the same film in the reduced state. The quantitative interpretation of these trends (1) from the acoustically thin to thick regime and (2) between different applied potentials will subsequently be used to extract polyaniline shear moduli as functions of film thickness and redox state.

Figure 2 shows the coulometric (panel a: charge, Q/mC) and acoustic (panel b: frequency change, $-\Delta f$/kHz) responses as functions of time (t/s) during film deposition. The charge response (panel a) comprises two components. One is an oscillatory component, which is associated with the reversible redox switching of the film; this component naturally increases in magnitude during the experiment. The second is a monotonically rising component, which is associated with the irreversible polymerization and deposition of the film. Interestingly, this component is initially linear but, after approximately 10 cycles, increases as a sharper function of time. This is consistent with the self-catalytic behaviour of polyaniline growth reported in the literature [11, 35–37] and may reflect an increase in surface area associated with a rough film [38]. The corresponding frequency change (panel b) as a function of time similarly shows two components, one associated with film deposition per se and the other with redox switching of deposited material. The difference here is that the monotonic frequency response component associated with film growth is linear with time.

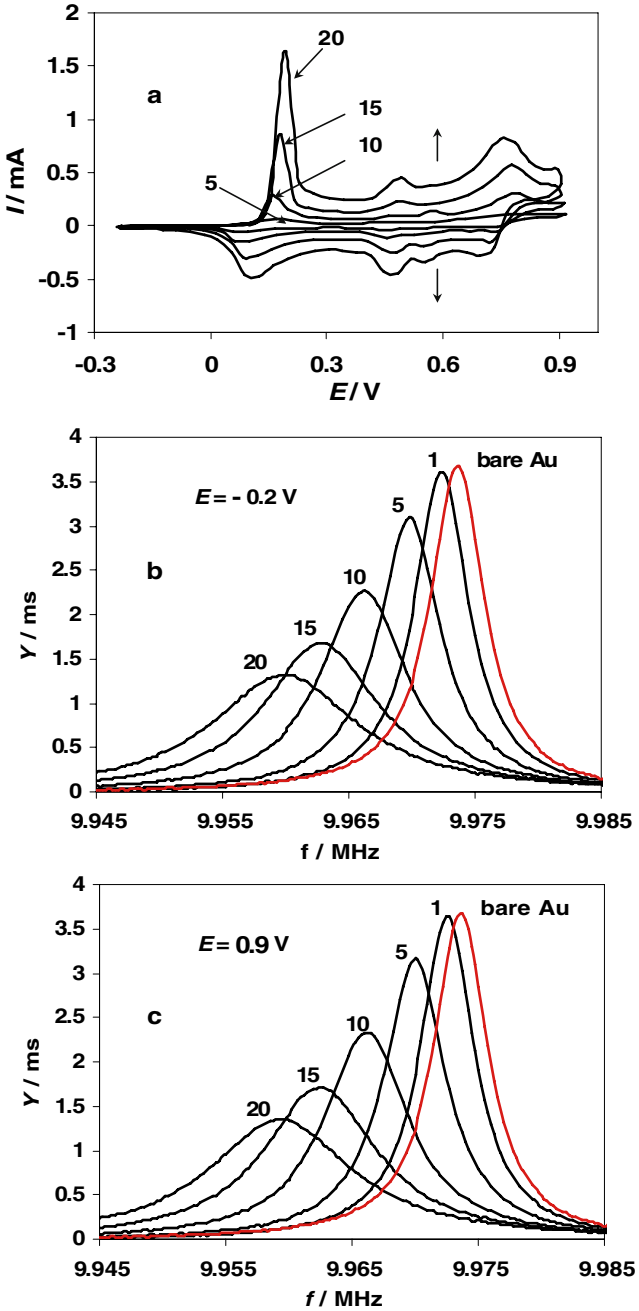

Fig. 1 Representative voltammetric experiment for deposition of a polyaniline film deposition from 0.1 M aniline/1 M $HClO_4$. **a** *i*–*E* curves for deposition cycles 5, 10, 15 and 20 (as annotated). Potential range: $-0.2 \le E/V \le 0.9$. Scan rate, v=10 mV s^{-1}. **b** Admittance spectra recorded at E=−0.2 V after each indicated potential cycle. *Spectrum at right hand side* (highest peak admittance) represents bare Au electrode, in solution, before film deposition. **c** As panel (**b**), but at the positive end of the indicated deposition cycle (E=0.9 V)

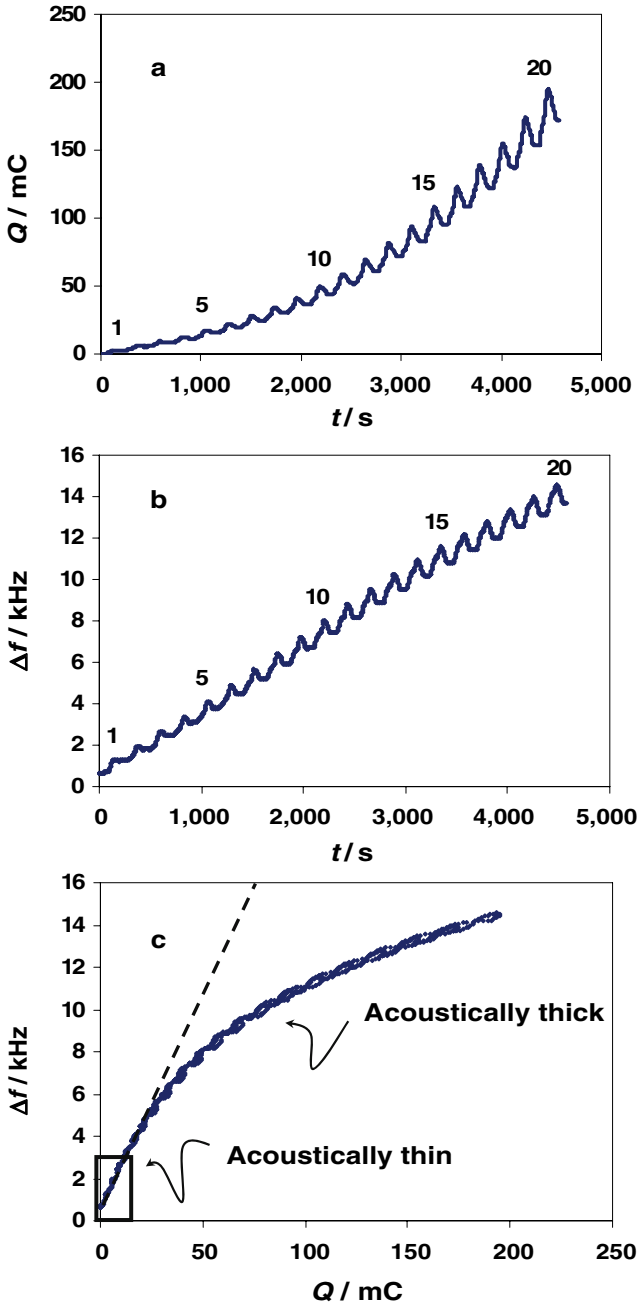

Fig. 2 EQCM charge (Q) and frequency shift (Δf) responses to polyaniline film deposition. **a** Q vs t response; *numbers* indicate deposition cycles. **b** Δf vs t response; *numbers* indicate deposition cycles. **c** Correlation of Δf vs Q; *rectangle* indicates regime for which viscoelastic parameters cannot be extracted. Data from experiment of Fig. 1

The hypothesis we now explore is that this distinction between the functional forms of the coulometric and acoustic responses is associated with viscoelastic effects. This is shown in panel c of Fig. 2, via direct correlation between the change in resonant frequency and the deposition charge. It is immediately apparent that the initial stages of film deposition are characterized by a linear Δf vs Q relationship. This is the acoustically thin regime, in which the frequency response is a gravimetric probe of the mass of film deposited (Δm/g). Combining the Sauerbrey equation:

$$\Delta f = -\left(\frac{2}{\rho_q v_q}\right) f_0^2 \frac{\Delta m}{A_p} = C_1 \Delta m \tag{10}$$

(where $C_1 = -2.26 \times 10^8$ Hz cm^2 g^{-1} represents the combination of quartz and crystal constants) with Faraday's law, the mass vs charge relationship yields the equivalent molar mass of deposited polymer, M/g mol^{-1}:

$$M = \frac{nFA_e}{Q} \frac{\Delta f}{C_1} \tag{11}$$

Using the data in Fig. 2 at $E = -0.2$ V (reduced film) at short times (within the box labelled "acoustically thin" in panel c), we find $M = 93.8$ g mol^{-1}. This is close to the molar mass of an aniline unit.

At longer times (higher deposition charge), the frequency response departs from the limiting linear relationship found at low charge. This signals a shift to a viscoelastically controlled frequency response, quantified via the fuller interpretation of Eq. 5 in the next section. As a final observation, the gravimetric nature of the short time (low charge) response is confirmed by the inability to make any physically meaningful fit to the viscoelastic model.

Evolution of shear modulus during polyaniline film growth

Having defined the regime where the EQCM response is viscoelastically controlled, we now focus on the determination of the shear modulus of the film. We explore two facets of the variations of G' and G'': evolution with the number of deposition cycles (effectively, film thickness) at a given potential, and variation with potential during a single deposition cycle.

Figure 3 shows values of G' and G'' at the extremes of the potential scan ($E = -0.2$ and 0.9 V) as functions of the growing film thickness, determined by the optimization procedure described earlier. AFM images of films were consistent with the shear modulus protocol optimized film thickness values; these images also revealed some surface roughness, so the values found should be regarded as effective averages, consistent with ideas advanced for poly (3,4-ethylenedioxythiophene) (PEDOT) films [38]. The vertical dotted line represents the lower limit of film thickness ($h_f \approx 0.12$ μm) at which we were able to obtain physically meaningful shear modulus components; the area to the left of the line represents the acoustically thin regime, discussed above.

Both shear modulus components increase with film thickness, but the extent of this variation is somewhat different. The storage shear modulus, G', increases rather modestly (e.g. from 1.14×10^7 to 1.58×10^7 dyn cm^{-2} at

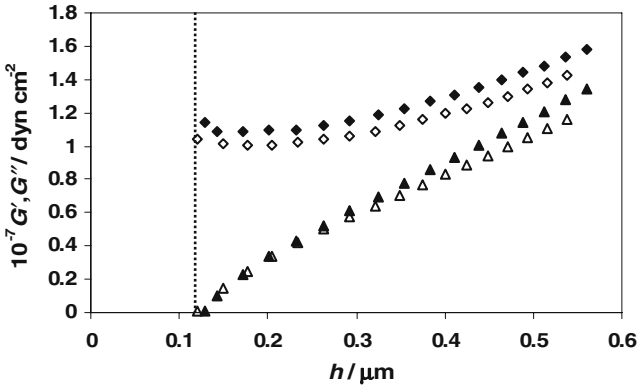

Fig. 3 Shear modulus component values as a function of film thickness. *Open symbols* $E=-0.2$ V; *filled symbols* $E=0.9$ V. *Diamond symbols* G'. *Triangle symbols* G''. *Vertical line* separate acoustically thin and thick regimes; *region to left of line* corresponds to the box in Fig. 2c. Data from experiment of Fig. 1

$E=0.9$ V). On the other hand, the loss shear modulus, G'', increases rather dramatically (e.g. from 8×10^4 to 1.34×10^7 dyn cm^{-2} at $E=0.9$ V). At the lower end of this range, we do not attribute great precision to the values, as it is our experience that, when the loss tangent (G''/G') is far from unity (i.e. outside the range $0.1<G''/G'<10$), the response is not particularly sensitive to the smaller of the two shear modulus components; in other words, the smaller component is not determined with precision. Nevertheless, the order of magnitude of G'' at short times is consistent with a liquid-like layer. The effect of further polymer deposition is to increase both components, but G'' far more dramatically. We speculate that there is some displacement of solvent by polymer, with the result that the loss tangent increases to values more typical of a bulk polymer material, to 0.81 at $E=-0.2$ V and 0.85 at $E=0.9$ V by the end of the experiment shown.

The systematically differing G' and G'' values at the extrema of the scans (see Fig. 3) suggest that there is merit in exploring the variations of these parameters with potential. The results of this more detailed study are shown in Fig. 4 at three selected stages of the deposition: just into the acoustically thick regime (5 cycles), in the middle of the range explored (9 cycles) and at the end of the experiment (20 cycles). For G'', particularly, the variations are generally much more subtle within a cycle (E-dependence) than between cycles (h_f-dependence). There is appreciable hysteresis in the plots, but this is at least in part due to the fact that there is more polymer present at any given potential during the cathodic half cycle than at the same potential during the preceding anodic half cycle; the end result is a gradual "ascent" up the y-axis.

Although the variations in G' and G'' values during a potential cycle are rather small (a few percent), they are nonetheless significant. As an example, consider the qualitative changes in G' during an anodic half cycle (Fig. 4,

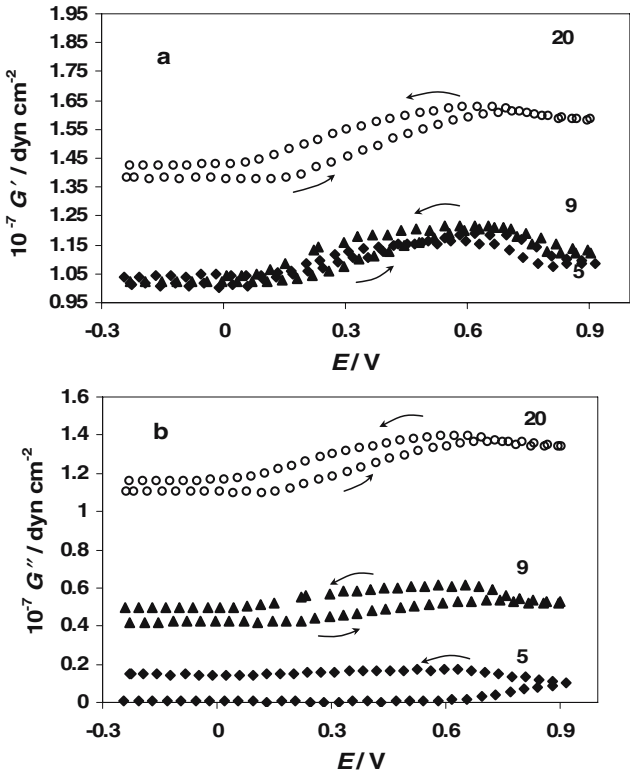

Fig. 4 Shear modulus components as functions of potential for deposition cycles 5, 9 and 20 (as indicated). **a** G′. **b** G″. *Arrows* indicate potential scan direction. Data from experiment of Fig. 1

panel a, cycle 20). The shear modulus is constant for $E<0.15$ V, starts to increase at $E\approx0.15$ V, peaks at $E\approx0.6$ V, then decreases slightly up to $E=0.9$ V. Comparing this with the current response in panel a of Fig. 1, we see that the increase is associated with the least anodic redox process and the decrease with the most anodic process; that is, there is a clear correlation of film dynamics with film composition. Similar effects have been observed during redox switching of layer-by-layer self-assembled films of a polymeric osmium complex [39]. We are pursuing the compositional aspects of this, particularly, in terms of spatial distributions of film components, in more detail using neutron reflectivity; this will be reported on subsequently.

The variations in shear modulus shown in Fig. 4 are made rather clearer by the differential presentational format of Fig. 5; to our knowledge, this approach has not been used previously. Although there is clearly some scatter in the data, the qualitative result is a pair of peaks (in opposite directions) in each half cycle at $E\approx0.2$ V and $E\approx0.75$ V, which coincide with the potentials of the first film redox peak and the onset of monomer oxidation, respectively (see Fig. 1, panel a). The response during the cathodic half cycle is a mirror image of the anodic response. The correlation of film mechanical properties with composition is unquestionable and suggests that this new presentational format may have considerable general utility.

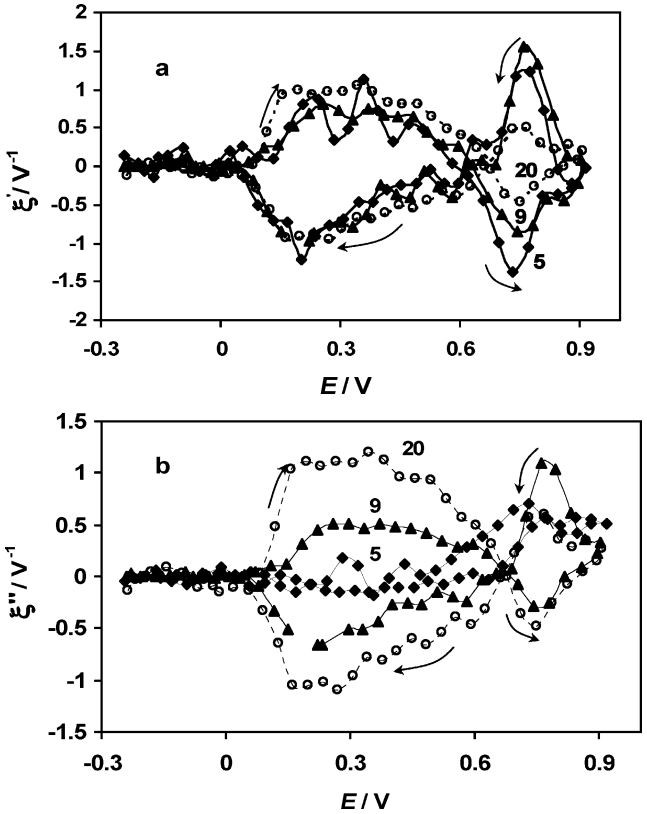

Fig. 5 Differential shear modulus components as functions of potential for deposition cycles 5, 9 and 20 (as indicated). **a** $\xi' = \frac{1}{G'_{(-0.2V)}}\frac{dG'}{dE}$ vs E. **b** $\xi'' = \frac{1}{G''_{(-0.2V)}}\frac{dG''}{dE}$ vs E. *Arrows* indicate potential scan direction. Data from Fig. 4

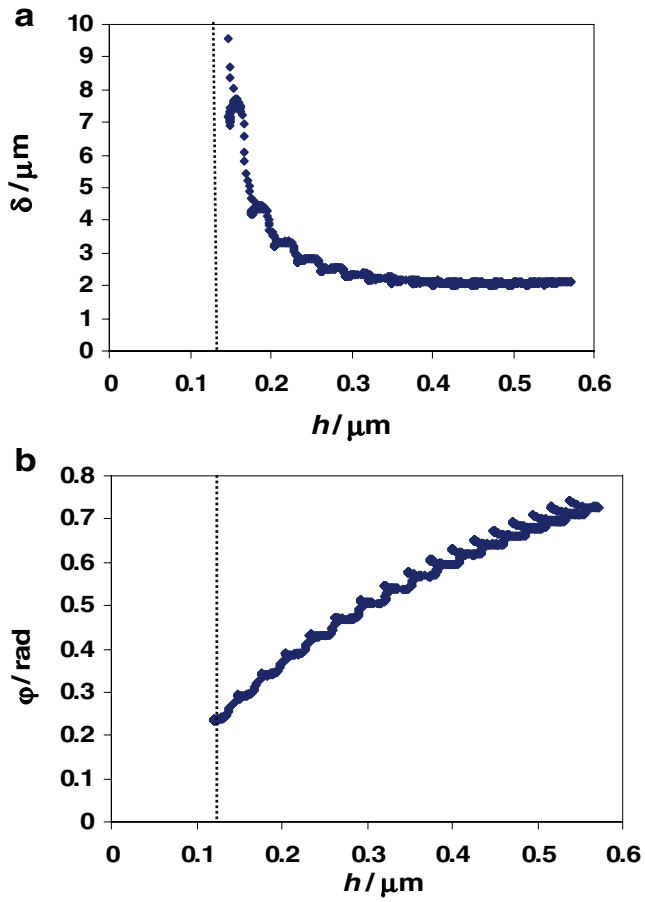

Fig. 6 **a** Decay length as a function of film thickness. **b** Acoustic wave phase shift as a function of film thickness. Data from experiment of Fig. 1, calculated using shear moduli of Fig. 3. *Vertical dotted line* as in Fig. 3

There is one interesting quantitative distinction between the storage and loss moduli. The relative changes in G' for the peak centred at E=0.2 V are relatively independent of film thickness (i.e. the curves for different numbers of deposition cycles superimpose) over a factor of about five variation in h_f. The corresponding changes in G'' increase substantially with film thickness. For both components, film thickness exerts an influence in the region of the second peak: the relative effect diminishes with increasing thickness. The compositional origins of the redox switching-driven changes will be explored in a future study of polyaniline films transferred to monomer-free solution (for which any possible complications of monomer oxidation and oligomer inclusion can be ruled out), but it is clear that electrostatic stiffening due to charge injection and solvent plasticization will be competing processes.

Further insight into the mechanics of the system can be obtained by consideration of the decay length (δ, defined by Eq. 9), and the acoustic phase shift across the film (ϕ, defined by Eq. 2). The former is a material property, and the latter is a property of both the material and of the sample, via film thickness. Using the shear modulus data of Fig. 3, we obtain the decay length and phase shift values shown in Fig. 6.

During the initial period of deposition, the values of the acoustic wave decay length (panel a) were very large; the vertical scale in Fig. 6 was chosen to allow better appraisal of the longer time data, but at the shortest times for which shear moduli were calculable δ>30 μm. This is a consequence of the low loss liquid-like nature of the film noted earlier. By the time the film thickness has grown to 0.2 μm, the decay length has fallen dramatically to 3.3 μm; thereafter, it approaches a steady state ("bulk") value of about 2 μm. As the decay length is always significantly larger than the film thickness throughout the experiment (h_f=0.57 μm at the end of the representative experiment shown), we never enter the semi-infinite regime; the model and analysis used are, therefore, appropriate.

The acoustic phase shift (Fig. 5, panel b), on the other hand, steadily increases with the film thickness. The key observation is that, over the interval shown, it remains in the optimal range for shear modulus determination. In particular, it does not approach the value of $\pi/2$ associated with film resonance. Again, the modelling protocol is validated.

Conclusions

Use of the full frequency response (admittance spectrum) of a thickness shear mode acoustic resonator allows one to follow the extent of electrodeposition and the viscoelastic properties of polyaniline films. In the present study, using a potentiodynamic control function and perchloric acid electrolyte, the admittance spectra allow one to observe the transition from acoustically thin films at low deposition charge to acoustically thick films at high deposition charge. In terms of film thickness, the boundary between the two was at a film thickness of about 0.12 μm for a 10-MHz resonator; the single shot nature of a deposition experiment does not allow exploration of the frequency regime within a single experiment. Values of acoustic decay length (a material property) and acoustic phase shift (a function of film properties and film thickness), subsequently calculated using the shear moduli resulting from the full analysis, validate the identification of this distinction.

Frequency shift data within the acoustically thin film regime, associated with negligible energy dissipation, can be interpreted gravimetrically via the Sauerbrey equation. Frequency responses within the acoustically thick film, associated with significant energy dissipation (decreased peak admittance), were interpreted viscoelastically. In this latter case, acoustic admittance spectra acquired as a function of potential (20 mV intervals) for multiple (typically 25) deposition cycles were acquired. The outcome was a set of film shear storage and loss moduli as functions of potential (within a given deposition cycle) and number of deposition cycles.

At a fixed potential, represented by the negative or positive extreme of the deposition cycle, the storage modulus increases modestly (over the range of about 1.1–1.6×10^7 dyn cm^{-2}) with film thickness. Simultaneously, the loss modulus increases more dramatically (over the range of about 0.008–1.3×10^7 dyn cm^{-2}). Qualitatively, this is consistent with a matrix that shifts from being liquid-like to viscoelastic.

Within a given deposition (and redox) cycle there are more subtle, but highly reproducible, variations in shear modulus components. By presenting these in a novel differential (with respect to potential) format, we find two peaks in the response to potential, one of which correlates with the first redox process and the other of which correlates with further film oxidation and polymerization.

Acknowledgement M. M. thanks CARA for partial support for a studentship. We thank Dr. Igor Efimov for helpful conversations.

References

1. Xue H, Li C, Shen Z (2005) Biosens Bioelectron 20:2330
2. Jureviciute I, Malinauskas A, Brazdziuviene K, Bernotaite L, Salkus B (2005) Sens Actuators B Chem 107:716
3. Choi S-J, Park S-M (2002) J Electrochem Soc 149:E26
4. Baba A, Tian S, Stefani F, Xia C, Wang Z, Advincula RC, Johannsmann D, Knoll W (2004) J Electroanal Chem 562:95
5. MacDiarmid AG (1997) Synth Met 84:27
6. MacDiarmid AG, Epstein AJ (1989) Faraday Discuss Chem Soc 88:317
7. Miras MC, Barbero C, Kotz R, Haas O (1994) J Electroanal Chem 369:193
8. Bernard MC, LeGoff AH (2006) Electrochim Acta 52:595
9. Syed AA, Dinesan MK (1991) Talanta 38:815
10. Dinh HN, Ding J, Xia SJ, Birss VI (1998) J Electroanal Chem 459:45
11. Zotti G, Cattarin S, Comisso N (1988) J Electroanal Chem 239:387
12. Pruneanu S, Csahok E, Kertesz V, Inzelt G (1998) Electrochim Acta 43:2305
13. Ivanov VF, Gribkova OL, Novikov SV, Nekrasov AA, Isakova AA, Vannikov AV, Meshkov GB, Yaminsky IV (2005) Synth Met 152:153
14. Gabrielli C, Keddam M, Nadi N, Perrot H (2000) J Electroanal Chem 485:101
15. Orata D, Buttry DA (1987) J Am Chem Soc 109:3574
16. Keita B, Mahmoud A, Nadjo L (1995) J Electroanal Chem 386:245
17. Hillman AR, Mohamoud MA (2006) Electrochim Acta 51:6018
18. Koehler S, Bund A, Efimov I (2006) J Electroanal Chem 589:82
19. Hillman AR, Efimov I, Skompska M (2005) J Am Chem Soc 127:3817
20. Efimov I, Hillman AR (2006) Anal Chem 78:3616
21. Hillman AR, Efimov I, Skompska M (2002) Faraday Discuss 121:423
22. Hillman AR, Efimov I, Ryder KS (2005) J Am Chem Soc 127:16611
23. Mahmoud A, Keita B, Nadjo L (1998) J Electroanal Chem 446:211
24. Hillman AR, Jackson A, Martin SJ (2001) Anal Chem 73:540
25. Brown MJ, Hillman AR, Martin SJ, Cernosek RW, Bandey HL (2000) J Mater Chem 10:115
26. Bandey HL, Martin SJ, Cernosek RW, Hillman AR (1999) Anal Chem 71:2205
27. Martin SJ, Granstaff VE, Frye GC (1991) Anal Chem 63:2272
28. Lucklum R, Behling C, Cernosek RW, Martin SJ (1997) J Phys D Appl Phys 30:346
29. Granstaff VE, Martin SJ (1994) J Appl Phys 75:1319
30. Saraswathi R, Hillman AR, Martin SJ (1998) J Electroanal Chem 460:267
31. Hillman AR, Brown MJ (1998) J Am Chem Soc 120:12968
32. Bandey HL, Hillman AR, Brown MJ, Martin SJ (1997) Faraday Discuss Chem Soc 107:105
33. Lagier C, Efimov I, Hillman AR (2005) Anal Chem 77:335
34. Bauermann LP, Barlett PN (2005) Electrochim Acta 50:1537
35. Stilwell DE, Park S-M (1988) J Electrochem Soc 135:2254
36. Johnson B, Park S-M (1996) J Electrochem Soc 143:1269
37. Wei Y, Sun Y, Tang X (1989) J Phys Chem 93:4878
38. Arnau A, Jimenez Y, Fernandez R, Torres R, Otero M, Calvo EJ (2006) J Electrochem Soc 153:C455
39. Calvo EJ, Forzani E, Otero M (2002) J Electroanal Chem 538–539:231